



Effects of flexibility and entanglement of sodium hyaluronate in solutions on the entry flow in micro abrupt contraction-expansion channels

Hidema, Ruri
Oka, Taiki
Komoda, Yoshiyuki
Suzuki, Hiroshi

(Citation)

Physics of Fluids, 31(7):072005-072005

(Issue Date)

2019-07

(Resource Type)

journal article

(Version)

Version of Record

(Rights)

© 2019 Author(s). This article may be downloaded for personal use only. Any other use requires prior permission of the author and AIP Publishing. The following article appeared in Physics of Fluids 31(7), 072005 and may be found at <http://dx.doi.org/10.1063/1.5096781>

(URL)

<https://hdl.handle.net/20.500.14094/90006271>



Effects of flexibility and entanglement of sodium hyaluronate in solutions on the entry flow in micro abrupt contraction-expansion channels

Cite as: Phys. Fluids **31**, 072005 (2019); <https://doi.org/10.1063/1.5096781>

Submitted: 19 March 2019 . Accepted: 27 June 2019 . Published Online: 22 July 2019

Ruri Hidema , Taiki Oka, Yoshiyuki Komoda , and Hiroshi Suzuki



View Online



Export Citation



CrossMark

ARTICLES YOU MAY BE INTERESTED IN

[Resolving the three-dimensional structure of particles that are aerodynamically clustered by a turbulent flow](#)

Physics of Fluids **31**, 071702 (2019); <https://doi.org/10.1063/1.5110323>

[Relaxation time of dilute polymer solutions: A microfluidic approach](#)


Journal of Rheology **61**, 327 (2017); <https://doi.org/10.1122/1.4975933>

[Steady-state extensional viscosity of a linear polymer solution using a differential pressure extensional rheometer on a chip](#)

Journal of Rheology **62**, 1261 (2018); <https://doi.org/10.1122/1.5033499>

CAPTURE WHAT'S POSSIBLE

WITH OUR NEW PUBLISHING ACADEMY RESOURCES

Learn more 



Effects of flexibility and entanglement of sodium hyaluronate in solutions on the entry flow in micro abrupt contraction-expansion channels

Cite as: Phys. Fluids 31, 072005 (2019); doi: 10.1063/1.5096781

Submitted: 19 March 2019 • Accepted: 27 June 2019 •

Published Online: 22 July 2019



Ruri Hidema,^{a)} Taiki Oka, Yoshiyuki Komoda, and Hiroshi Suzuki

AFFILIATIONS

Department of Chemical Science and Engineering, Kobe University, Kobe 657-8501, Japan

^{a)} Author to whom correspondence should be addressed: hidema@port.kobe-u.ac.jp. Tel.: +81-78-803-6657. Fax: +81-78-803-6657.

ABSTRACT

In this study, the effects of polymer flexibility and entanglement on elastic instability were investigated by observing sodium hyaluronate (hyaluronic acid sodium salt, Na-HA) solution in planar abrupt contraction-expansion microchannels. As the rigidity of Na-HA depends on the ionic strength of a solvent, Na-HA was dissolved in water and phosphate buffered saline with concentrations from 0.15 wt. % to 0.45 wt. %. The rheological properties were measured and analyzed to detect the Na-HA overlap and entanglement concentrations. The flow regimes of the Na-HA solutions in several planar abrupt contraction-expansion channels were characterized in the Reynolds number and Weissenberg number space. The effects of the solvent, solution concentration, and channel geometry on the elastic corner vortex growth curve and flow regimes characterized by the Weissenberg number were analyzed. It was found that the entanglement of Na-HA in the solution is a more dominant factor affecting the flow regimes than the solution relaxation time and polymer rigidity.

Published under license by AIP Publishing. <https://doi.org/10.1063/1.5096781>

I. INTRODUCTION

Nonlinear flow behavior of viscoelastic fluids, such as aqueous polymer solutions and polymer melts, in abrupt contraction flows has been a common topic for many years.^{1–12} Historically, the investigation of such flows was initiated to control the extrusion die of polymer melts in industrial processes.¹³ In the last decades, flow behavior of polymer solutions in microscales has attracted significant attention because it is related to many industrial applications, such as ink-jet printing, fiber spinning, micromixing, lab-on-a-chip techniques, and microrheometry.^{14–25}

A number of studies on aqueous polymer solutions have been conducted through contraction/contraction-expansion flows.^{7,12,14–17,26–39} When viscoelastic solution flows through a contraction throat, different characteristic flow regimes may appear in the upper stream region of the contraction throat with the increasing flow rate. Lip vortices, elastic corner vortices, diverging flows, and time-dependent unstable flows were observed in contraction channels.^{7,12,14} Flow regimes may be characterized by the Weissenberg number, $Wi(-)$, which is determined by elasticity. Particularly,

in microscale, high Wi at a low Reynolds number, $Re(-)$, can cause elastic instability because of a high elasticity number, $El(-) = Wi/Re$, which is the ratio of elasticity and inertia.^{14,40–45} Therefore, the flow regimes of viscoelastic polymer solutions in microcontraction/contraction-expansion channels are often categorized in the $Wi-Re$ space. The flow develops along the slope of El in the $Wi-Re$ space.¹⁴ However, as the flow regimes and development of the corner vortices are affected by many factors, $Wi-Re$ space cannot capture all the details of the flow characteristics. Not only the effects of inertia and elasticity but also the effects of channel geometry and polymer rigidity are required to be considered.^{17,33,35}

The contraction ratio, $\beta(-)$, of contraction/contraction-expansion channels is an important factor affecting the flow. Evans and Walters⁴⁶ and Chiba *et al.*^{9,10} studied the vortex enhancement in Boger and shear-thinning fluids in planar and square-square contraction channels. In the work of Evans and Walters,⁴⁶ the effects of different contraction ratios ($\beta = 4, 16$, and 80) on the vortex enhancement were considered in both planar and square-square contraction channels. In planar contraction channels, vortex activity of Boger fluids was reduced for all values of β . Conversely,

shear-thinning fluid exhibited vortex enhancement. The shear-thinning fluid in large- β channels ($\beta = 16$ and 80) induced a lip vortex, and it grew as a dominant corner vortex. However, in a channel with $\beta = 4$, the lip vortex did not appear. In a square-square contraction channel, Boger fluids induced strong vortex enhancement. Given that these studies were published, the effects of β and viscoelastic properties of fluids on the appearance of the lip vortex have been extensively studied. Rothstein and McKinley^{11,12} observed vortex enhancement in a Boger fluid in axisymmetric contraction-expansion channels. The lip vortex appeared in a channel with $\beta = 2$, but it did not appear in channels with $4 \leq \beta \leq 8$, when only the corner vortex appeared. Alves *et al.*^{27,28,47} studied the effects of β and viscoelastic fluid properties on the vortex development. The appearance of the lip and salient corner vortices and their development to the corner vortices are affected by β and the Deborah number. In the contraction channel with $\beta = 4$, a lip vortex was not visible, and a salient corner vortex developed to the corner vortex with the increasing Deborah number. The lip vortex evolution to the corner vortex was observed in the channels with $\beta = 20$ and 100 with the increasing Deborah number. Strong lip vortices with the vortex centers located close to the smaller-channel entrance is the feature of higher- β channels. More recently, Lanzaro and Yuan³⁶ studied the effects of β on a shear-thinning solution in abrupt contraction-expansion microchannels. The strong lip vortex appearance in microchannels was similar to that in the previous studies. Symmetric and stable corner vortices appeared in the channels with $\beta = 4$ at moderate El , and symmetric lip vortices or single lip vortices appeared in the channels with $\beta = 8$ and 16 .

The corner vortex size development was also studied in different channel geometries. Rodd *et al.*¹⁴ quantified the inertio-elastic vortex growth in a dilute polyethylene oxide solution in microchannels with $\beta = 16$. The dimensionless vortex size, L_v/w_u , which is the corner vortex length, L_v (m), divided by the width of the upper stream channel, w_u (m), was plotted as a function of Wi . When the elasticity number was tuned as $3.8 \leq El \leq 89$, the dimensionless vortex length collapsed into a single almost linear curve. The linear behavior of the dimensionless vortex size independent on El was also confirmed in the work of Lanzaro and Yuan.³⁶ They compared the curves of L_v/w_u in the channels with $\beta = 4$ and 8 and found nearly linear dependence on Wi , which was not affected by El .

At the same time, the independence of L_v/w_u from β and El is not a universal property, as it is affected by the aspect ratio of a channel. It was reported that the vortex size was smaller in a planar channel than in an axisymmetric channel with the same contraction ratio β .^{1,12,14,15} In microscale, it was confirmed using the growth curve of L_v/w_u observed by Lanzaro and Yuan,³⁶ who showed that the smaller aspect ratio induces the larger corner vortex. The aspect ratio, $\alpha = h/w_u$, is defined as the depth of the channel, h (m), divided by w_u . The effect of α on the corner vortex enhancement is more pronounced than the effect of β . In addition, it was shown that the vortex growth at smaller α is sensitive to El .³⁶

In abrupt contraction or contraction-expansion microchannels, the length of the constriction channel, L_c (m), also affects the corner vortex size and stability. Rodd *et al.*¹⁷ examined the effect of increasing L_c on the flow regimes in an upstream of an abrupt contraction-expansion channel with $\beta = 16$. When Re and Wi remained constant, the lip and elastic corner vortices disappeared,

the flow became nonsymmetric, and the streak lines became more chaotic with increasing L_c . It was explained by the effects of inertia on the flow, which became important with increasing L_c . However, not only the effects of L_c and El but also the polymer entanglement and relaxation time of the polymer solution are important for the flow characteristics.^{16,17,33}

The effects of polymer entanglement, stiffness, and distribution of molecular weight on the flow characteristics in contraction or contraction-expansion flows were discussed in several studies. Gulati *et al.*³¹ investigated the flow regimes of a semidilute deoxyribonucleic acid (DNA) solution in an abrupt planar contraction flow with $\beta = 2$. DNA is a relatively rigid polymer compared with flexible polyethylene oxide (PEO), and the relaxation time of DNA solution is greater. Therefore, El reaches very high values in the experiments, which induces the rapid increase in the corner vortices' size at lower Wi . However, in the work of Gulati *et al.*,³¹ lip vortices were not observed; only the corner vortex appeared. Miller and Cooper-White¹⁶ studied the effects of chain conformation of polymers on the elastic instability in polymer-surfactant systems. Polymer chains become relatively rigid when aggregating with the surfactant. Thus, it was found that the rigid polymer-surfactant conformation induces either the flow transition from laminar flow to the elastic corner vortex or the transition from the corner vortex to the unstable flow at lower Wi values compared with flexible polymers. Li *et al.*³⁵ studied the effects of polydispersity of polymers on their extensional viscosity and flow regimes in abrupt contraction-expansion flows. Evidently, the high molecular weight of polymers in the molecular distribution affects the flow. Omowunmi and Yuan³³ questioned the validity of the calculation of physical properties of a sample solution, such as Wi or El , with a single relaxation time. Although several previous studies stated the importance of flexibility and entanglement of polymers on the flow regimes, it has not been fully clarified yet.

In this study, we measured the flow characteristics of the sodium hyaluronate (hyaluronic acid sodium salt, Na-HA) solution in planar abrupt contraction-expansion microchannels to clarify the effects of polymer flexibility and entanglement on the flow. Hyaluronic acid (HA) is a high-molecular weight glycosaminoglycan.^{48–50} As the HA molecules are bounded by water, the volume occupied by each chain becomes very large in water solution. The effective spherulike volume of an HA molecule in a good solvent grows approximately as $M^{1.8}$, where M is the molecular weight.⁵⁰ As the viscoelastic properties of human synovial fluids are attributed to the HA, the rheological properties of the HA solution have been intensively studied.^{51–55} HA solutions show shear-thinning behavior and strain-hardening under extensional deformations.^{53,54} HA forms a loosely entangled network, and the rheological behavior of HA is significantly affected by its concentration and molecular weight.^{48,50} The ionic strength of a sample solution is also a very important factor governing the rheological properties. The reason is that the rigidity of Na-HA molecules is affected by the ionic strength of the solution. The persistent length and excluded volume of Na-HA expand with the increase in ionic strength.^{52,56,57}

In this study, we dissolved Na-HA in water and Dulbecco's phosphate buffered saline (PBS) and observed the flow regimes in microchannels. Several types of channels were prepared to compare the effects of β , α , and L_c . As the ionic strength is different in water

and PBS, Na-HA behaves as a semiflexible linear polymer in water and as a flexible polymer in a PBS solution. The viscoelasticity and Na-HA conformation were controlled by varying the concentration and solvents. Finally, the effects of the polymer stiffness and entanglement on the elastic unstable flows in microchannels with several geometries were studied beyond the elasticity number.

II. EXPERIMENTAL PROCEDURES

A. Materials

Hyaluronic acid sodium salt (Na-HA, Wako, hyaluronic acid sodium salt from *streptococcus zooepidemicus*, $M_w \sim 1$ MDa) was dissolved in distilled water and Dulbecco's PBS with concentrations from 0.15 wt. % to 0.45 wt. %. The Dulbecco's PBS contained NaCl at 137 mM, KCl at 2.68 mM, Na_2HPO_4 at 10.1 mM, and KH_2PO_4 at 1.76 mM. Solutions were mixed for 24 h at 25 °C with low speed to avoid breaking of molecules.

Flow fields of Na-HA solution were visualized by bright-field and fluorescent modes of a microscope. Prior to the bright field experiments, polystyrene particles with a diameter of 2.11 μm were seeded in the sample solutions at the concentration of 0.1 wt. % for the flow visualization. Sodium dodecylbenzenesulfonate (SDBS) was also added at 0.2 wt. % to prevent adhesion of particles to other particles or to the channel walls. The critical micelle concentration of SDBS in de-ionized water is about 4.0×10^{-4} M (~ 0.014 wt. %).^{58,59} We confirmed that the concentration of 0.2 wt. % SDBS did not affect the flow of Na-HA solution. The solution with polystyrene particles was remixed for 1 h with low speed. In the case of fluorescent streak imaging, 0.2 wt. % SDBS was dissolved, and Rhodamine 6G particles with a diameter of 2.0 μm were seeded in the Na-HA solution.

B. Viscosity and relaxation time measurements

The viscosities of the Na-HA solutions were measured using a rheometer (MCR301: Anton Paar) with a cone-plate device. The diameter of the cone-plate device was 50 mm, and the cone angle was 0.04 rad. The shear rates were varied from 1 to 1000 s^{-1} , and slip effects on the surface were not observed. The relaxation times of the solutions were measured by using a capillary breakup extensional rheometer (Thermo Scientific HAAKE, CaBER).^{60–64} The CaBER can measure the relaxation time of a sample solution under uniaxial extension. The relaxation time measured by CaBER in the elasto-capillary thinning region is related to the longest relaxation time of an elongated polymer.^{60–64} The elastic instability in microfluidics is affected by extensional properties of the solution; therefore, the relaxation time measured by CaBER is adopted as a relaxation time of the solution. The sample solution was inserted between the two sample plates of the CaBER. The diameter of the two sample plates was 6 mm. The two sample plates were expanded from an initial gap of 3 mm to a final gap in 0.05 s. The final gap was 9 mm for Na-HA PBS solution and was 10 mm for Na-HA water solution. The final gap was varied to achieve the elasto-capillary thinning of each sample solution. As described in Sec. III C, Na-HA water solution is more viscoelastic than Na-HA PBS solution; therefore, the final gap was wider for the measurements of Na-HA water solution. After the rapid expansion, the two plates were maintained at the final spacing. The liquid column of the sample solution was thinning over time.

The time dependence of the diameter of the liquid column, $D(t)$ (m), was measured, which was used to calculate the relaxation time of the sample solution, λ (s). The examples of $D(t)$ of different solutions are shown in Fig. 3; $D(t)$ in the elasto-capillary thinning region decays exponentially in time, t (s), as described by $D(t) \propto \exp(-t/3\lambda)$. λ is related to the longest relaxation time of Na-HA in each sample solution.

C. Flow observations in microchannels

Figure 1(a) shows a schematic of a planar micro abrupt contraction-expansion channel used in this study. The channel was made of polydimethylsiloxane (PDMS) attached to a glass plate, as shown in Fig. 1(c). Four different channels with different geometries were prepared. The width at the contraction part, w_c (m), and the width at the upstream, w_u (m), of the channels were different. Thus, the contraction-expansion ratio, β (-), and the aspect ratio, $\alpha = h/w_u$, of the channels were variable. The lengths of the contraction part, L_c (m), were also different. The depth of all channels, h (m), was 50 μm . The details are shown in Table I.

A microscope (Olympus, IX83) was used to observe flows in these planar micro abrupt contraction-expansion channels, as shown in Figs. 1(c) and 1(d). Sample solutions were injected from a tube connected to a syringe, and the syringe driver controlled the flow rates. The entry flows in the upstream region to the contraction part were visualized by both bright field and fluorescent modes of the microscope. A digital video camera (Panasonic, HC-W850M) and a high-speed video camera (IDT Japan, Inc., Os8-S1) were used to record the flow images. The exposure time was controlled to detect the flow characteristics. The flow observation of each solution at each flow rate was repeated at least 5 times and more in order to confirm the reproducibility.

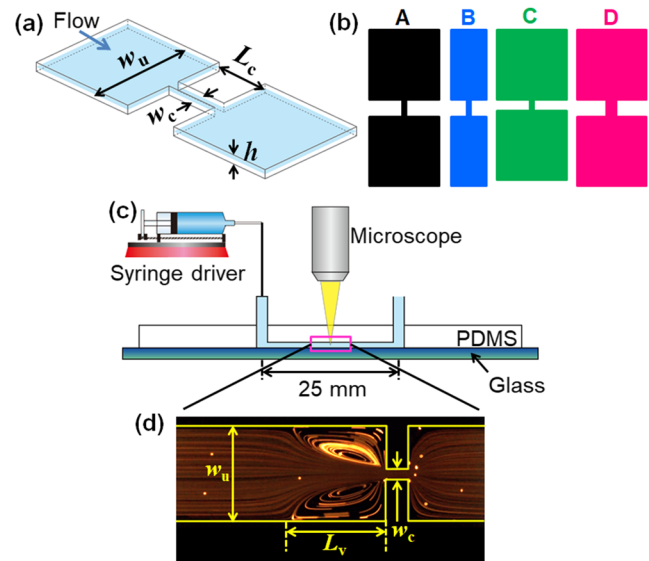


FIG. 1. Schematics of the planar micro abrupt contraction-expansion channels [(a) and (b)] and experimental apparatus (c). Example of a fluorescent streak image obtained in the experiment (d). Vortices in the upper stream region are characterized by the vortex length L_v (m).

TABLE I. Geometric parameters of the channels.

	w_u (μm)	w_c (μm)	L_c (μm)	h (μm)	α (-)	β (-)
Channel A	400	25	100	50	50/400	16:1:16
Channel B	200	25	100	50	50/200	8:1:8
Channel C	400	25	50	50	50/400	16:1:16
Channel D	400	50	100	50	50/400	8:1:8

D. Characterizing the flow

To characterize the entry flows, the following dimensionless numbers were used: Reynolds number, Re (-), Weissenberg number, Wi (-), and elasticity number, El (-). These parameters are defined by Eqs. (1)–(3).¹⁴ Re is identified as the ratio of inertial to viscous forces.^{42,43} Re is calculated with the average velocity in the contraction part, \bar{V}_c (m/s) = $Q/(w_c h)$, and hydraulic diameter, D_h (m) = $2hw_c/(w_c + h)$,

$$Re = \frac{\rho \bar{V}_c D_h}{\eta_0} = \frac{2\rho Q}{(w_c + h)\eta_0}. \quad (1)$$

Here, ρ (kg/m³) is the density of the solution, η_0 (Pa s) is the zero-shear viscosity, and Q (m³/s) is the flow rate. Wi is the ratio of two time scales that is the relaxation time, λ , and characteristic residence time in the contraction throat. The characteristic residence time is defined as $l/\bar{V}_c \approx \dot{\gamma}_c^{-1}$, where l (m) is the characteristic length scale.^{42,43} At the same time, Wi is identified as the dimensionless strain rate^{42,43}

$$Wi = \lambda \dot{\gamma}_c = \frac{\lambda \bar{V}_c}{w_c/2} = \frac{2\lambda Q}{hw_c^2}. \quad (2)$$

The elasticity number, El (-), is defined as the ratio of Wi to Re . El is the ratio of elastic to inertial stress, which provides a measure of the relative importance of elastic stress in comparison with inertial stress. El is independent of the fluid kinematics and represents the trajectory of a set of experiments with a sample solution in Wi – Re space.^{42,43} Thus, El is used to capture the characteristics of inertio-elastic or elastic instabilities,

$$El = \frac{Wi}{Re} = \frac{\lambda \eta_0 (w_c + h)}{\rho w_c^2 h}. \quad (3)$$

To describe the vortex growth in the entry flows, a dimensionless vortex length L_v/w_u (-) is introduced, where L_v (m) is the vortex length defined in Fig. 1(d).

III. RESULTS AND DISCUSSIONS

A. Rheological properties of the fluids

Shear viscosities, η (Pa s), of Na-HA water and PBS solutions with the concentrations from 0.15 to 0.45 wt. % are shown in Figs. 2(a) and 2(b). All the Na-HA solutions show shear-thinning behavior at a high shear rate. Na-HA water solutions show higher shear viscosities than Na-HA PBS solutions. The increase in the Na-HA concentration in the PBS solutions from 0.15 to 0.45 wt. % results in an increase in η_0 and more pronounced shear-thinning behavior. Rheological properties of Na-HA water and PBS solutions were measured in many previous studies.^{46,51,52} The morphology of Na-HA in solution is affected by the ionic strength of the solution.^{49,50,54,55} Na-HA is a semiflexible polymer in water solution and a flexible polymer in PBS solution at the ionic strength of 0.15M, which affects the excluded volume. Na-HA molecules are in

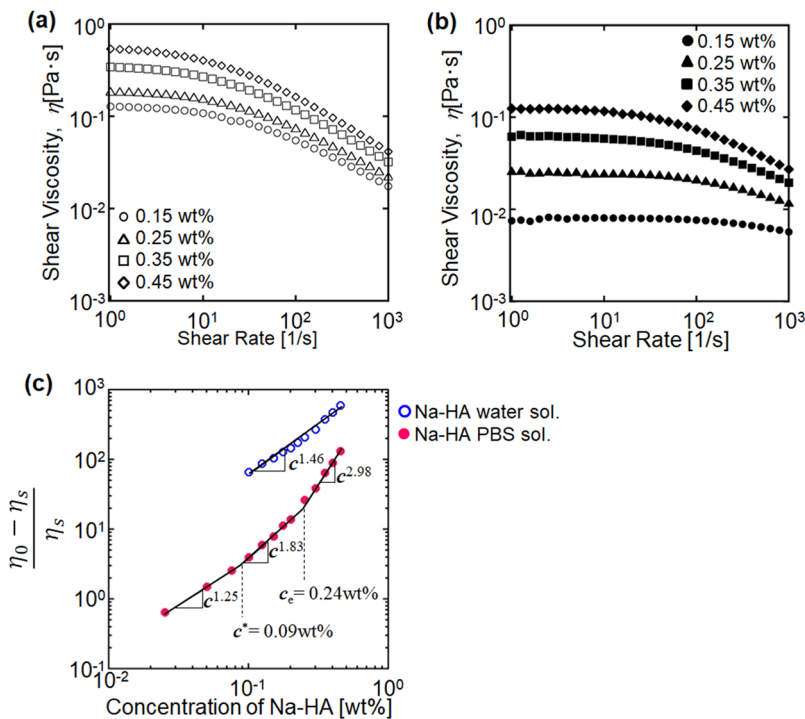


FIG. 2. (a) Shear viscosity of Na-HA water solution, (b) shear viscosity of Na-HA PBS solution, and (c) zero-shear specific viscosity of Na-HA water and PBS solutions.

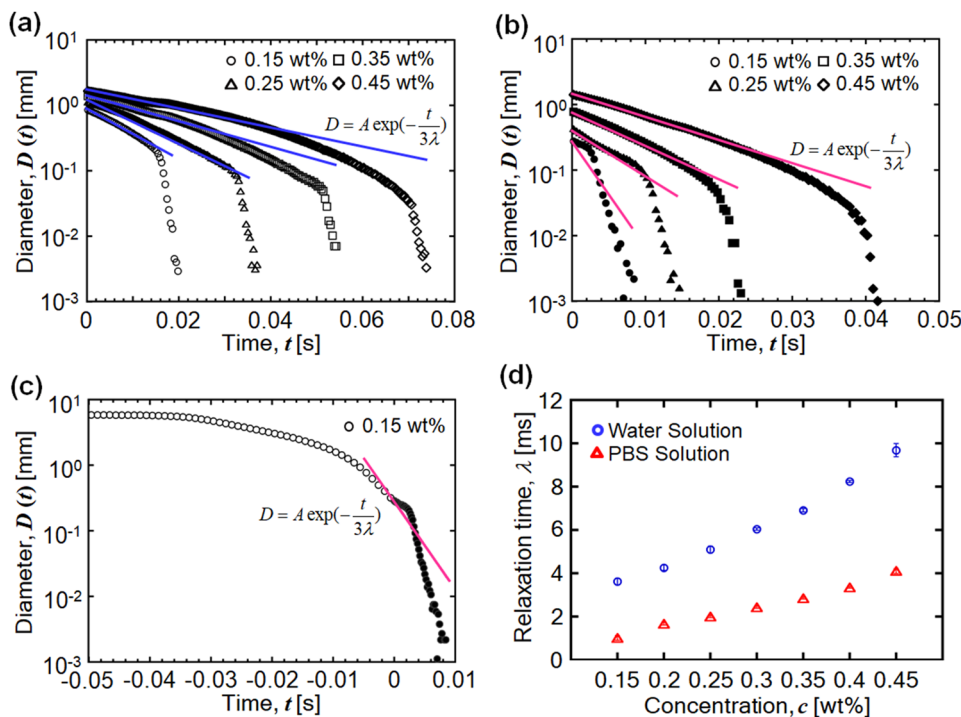


FIG. 3. (a) Time dependence of the liquid column diameter, $D(t)$, of Na-HA water solution, which was fitted by the function, $D(t) \propto \exp(-t/3\lambda)$.^{60,61,64} (b) $D(t)$ of Na-HA PBS solution. (c) Superposition of the fitting curve to $D(t)$ of Na-HA 0.15 wt. % PBS solution before $t = 0$. (d) Relaxation time of the considered sample solutions.

an extended state in water and in a relatively shrink state in PBS, which affects the shear viscosity.^{50,54,55} Zero-shear specific viscosity, $\eta_{sp}(-)$, which is defined with η_0 and the solution viscosity η_s (Pa s), as $\eta_{sp} = (\eta_0 - \eta_s)/\eta_s$ [Fig. 2(c)], of Na-HA water and PBS solutions was used to find the overlap concentration, c^* (wt. %), and entanglement concentration, c_e (wt. %).^{49,50} $\eta_{sp}(-)$ of Na-HA water and PBS solutions obtained in the present study shows a good agreement with the previous studies. In the case of Na-HA PBS solution, the overlap concentration was found as $c^* \sim 0.09$ wt. %, and the entanglement concentration was found as $c_e \sim 0.24$ wt. %. Thus, the Na-HA PBS solutions with the concentrations from 0.15 to 0.45 wt. %, which were observed in the present study, are in semidilute-unentangled and semidilute-entangled states. In the case of Na-HA water solution, based on the overlap criterion ($c^*\eta \sim 1$) and scaling prediction proposed in the previous studies, the solutions with the concentrations from 0.15 to 0.45 wt. % are in the semidilute-unentangled state. However, the effect of entanglement was slightly detected in η_{sp} at 0.40 and 0.45 wt. % of Na-HA water solution [Fig. 2(c)].

The relaxation times of the sample solutions are shown in Fig. 3(d). As was described above, the relaxation time of the solution was calculated by fitting the time dependence of the liquid column diameter $D(t)$ (m) in the elasto-capillary thinning region with a fitting function $D(t) \propto \exp(-t/3\lambda)$. Figures 3(a) and 3(b) show the examples of $D(t)$ of Na-HA water and PBS solutions. In Fig. 3(b), the fitting function does not seem to fit well to $D(t)$ of Na-HA 0.15 wt. % PBS solution. This is because Na-HA 0.15 wt. % PBS solution is less viscous, and thus, the elasto-capillary thinning region starts before $t = 0$ when the two sample plates of CaBER reach the final position. It is confirmed in Fig. 3(c) by superposing the fitting curve of Na-HA

0.15 wt. % PBS solution to $D(t)$ before $t = 0$. $t = -0.05$ corresponds to the time when the sample plates start to move. The relaxation time of Na-HA water solution is higher than that of Na-HA PBS solution at similar concentrations. The relaxation time tends to increase, when the concentration of Na-HA is increased. Na-HA water solution is more viscoelastic than Na-HA PBS solution. The density, the zero-shear viscosity, and the relaxation time are summarized in Tables II and III. These data were used to calculate dimensionless numbers.

B. Vortex growth and inertio-elastic instability in the channels

Figure 4 shows the flow regimes of Na-HA PBS solution at the concentration of 0.3 wt. % in channel (D). The contraction ratio of channel (D) is $\beta = 8$. Figures 4(1)–4(6) demonstrate the successive

TABLE II. Density and rheological properties of Na-HA water solutions.

Concentrations of Na-HA water sol. (wt. %)	ρ (kg/m ³)	η_0 (Pa s)	λ (ms)
0.15	1001.5	0.128	3.62
0.20	1002.0	0.132	4.26
0.25	1002.5	0.186	5.10
0.30	1003.0	0.246	6.04
0.35	1003.5	0.342	6.91
0.40	1004.0	0.425	8.24
0.45	1004.5	0.564	9.69

TABLE III. Density and rheological properties of Na-HA PBS solutions.

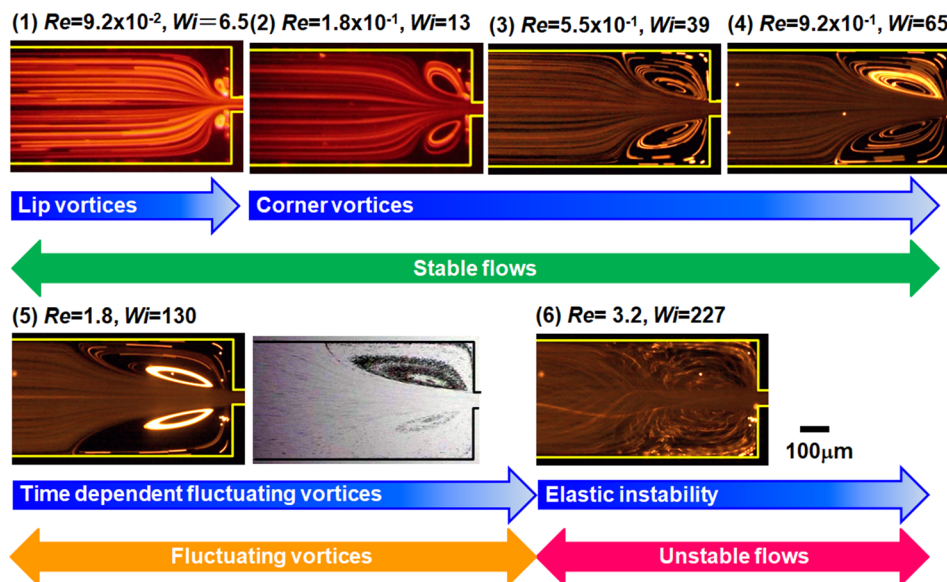
Concentrations of Na-HA PBS sol. (wt. %)	ρ (kg/m ³)	η_0 (Pa s)	λ (ms)
0.15	1001.5	0.008	1.01
0.20	1002.0	0.014	1.68
0.25	1002.5	0.024	2.00
0.30	1003.0	0.036	2.44
0.35	1003.5	0.060	2.85
0.40	1004.0	0.093	3.35
0.45	1004.5	0.126	4.11

increase in the flow rate, and, therefore, the increase in Re and Wi . When Wi is low, lip vortices appear at the entrance of the contraction throat [Fig. 4(1)]. The lip vortices at that condition are stable. With the increase in the flow rate, the lip vortices become larger and reach the sidewall of the upstream channel [Fig. 4(2)]. Then, the vortices grow along the edge of the upstream as the corner vortices [Figs. 4(3) and 4(4)]. In this flow-rate range, the vortices are stable and symmetric. With the further increase in the flow rate, the vortices continue to grow and begin showing time-dependent behavior when $Wi = 130$ [Fig. 4(5)]. The corner vortices become asymmetric and start fluctuating in time. Finally, the flow becomes unstable, as shown in Fig. 4(6). The typical flow regimes, namely, the lip vortices, corner vortices, time-dependent corner vortices, and unstable flow, were also observed at different concentrations of Na-HA PBS solutions in channel (D). Although the elasticity number in Na-HA water solution is much higher than that in Na-HA PBS solution, similar flow regimes were observed in Na-HA water solution in channel (D). The flow regimes were also similar in both PBS and water solutions in channels (A) and (C) with $\beta = 16$. In the case of channel (B) with $\beta = 8$, lip vortices were observed only at a very low flow

rate, Wi , and El of both water and PBS solutions. In channel (B), lip vortices instantly turn into corner vortices with the increase in the flow rate. It was reported that shear-thinning fluids and low β damp the lip vortices' formation.^{11,12,31,32} Therefore, stable lip vortices of highly shear-thinning and viscoelastic Na-HA solution were observed at very limited flow rates in channel (B). Channels (D) and (B) have the same β , but Wi and El of a solution flowing in channel (D) are lower because of the greater w_c . Thus, we could observe stable lip vortices in channel (D) up to relatively high flow rates.

To characterize the vortex growth in the entry flows, the dimensionless vortex length, L_v/w_u , was calculated. Figure 5(a) shows L_v/w_u of Na-HA water solution in different channels as a function of Wi/β . The vortices grow linearly when Wi/β is less than 10; then, the growth rate gradually decreases. The increase in the vortex size in channels (A), (C), and (D) followed the similar line. All these channels have the same aspect ratio α . The vortex growth curve in a certain channel, e.g., in channel (A), does not depend on the Na-HA concentration; however, the concentration slightly affects the maximum vortex size. It was reported that the shear-thinning properties lead to the increase in the vortex size.^{46,47} In this experiment, the shear-thinning properties were enhanced by increasing the Na-HA concentration; thus, the present study agrees with the previous studies in terms of the final vortex size. Although the tendencies of the vortex growth in Na-HA water solution in channels (A), (C), and (D) were similar, in channel (D), the vortex growth was maintained up to higher flow rates and values of Wi . The corner vortex in Na-HA water solution in channel (D) with lower contraction ratio $\beta = 8$ was stable.

In channel (B), $\beta = 8$, which is the same to channel (D); on the other hand, the aspect ratio α is 50/200, which is larger than that of the other channels, 50/400, and the vortex was larger compared with the other channels. It was reported that the vortex size is larger in axisymmetric channels than in planar channels.^{14,15} Therefore, it is reasonable to consider that the larger aspect ratio induces the increase in the vortex size.

**FIG. 4.** Entry flows of Na-HA PBS solution at the concentration of 0.3 wt. % in channel (D) with the flow rates of (1) 0.6 ml/h, (2) 1.2 ml/h, (3) 3.6 ml/h, (4) 6.0 ml/h, (5) 12 ml/h, and (6) 21 ml/h. Re and Wi are indicated in the figure, and $El = 71$. When Wi is low, lip vortices appear (1); with the increase in Wi , the vortices grow [(2)–(5)] and finally turn to unstable flows (6).

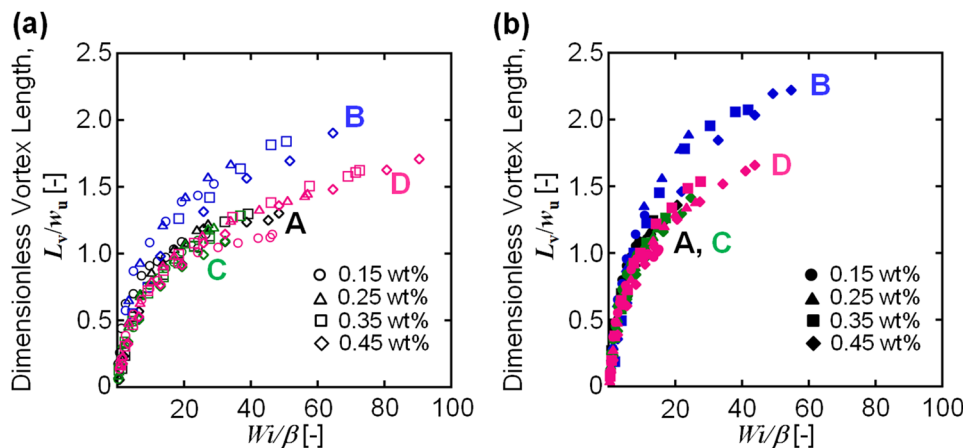


FIG. 5. Dimensionless vortex length L_v/w_u (-) of (a) Na-HA water solution and (b) Na-HA PBS solution as a function of Wi/β . A–D in the figures indicate channels (A)–(D), respectively.

Figure 5(b) shows the vortex growth in Na-HA PBS solution in different channels. The tendency of the vortex growth is similar to that of Na-HA water solution. In the case of Na-HA PBS solution, it looks that the vortices grow faster at lower Wi/β . This is due to the lower relaxation time of Na-HA PBS solution to calculate Wi , which is about 1/3 of the relaxation time of Na-HA water solution. Therefore, if we compare the vortex growths of Na-HA water and PBS solutions by flow rates of each solution, the vortices of Na-HA water solution grow faster at lower flow rates. The viscoelasticity of Na-HA water solution enhances the vortex growth.

C. Flow regimes on Wi - Re phase diagram

Figures 6 and 7 show the Wi - Re space of Na-HA PBS and water solutions, which summarizes the flow regime in channels (A)–(D).

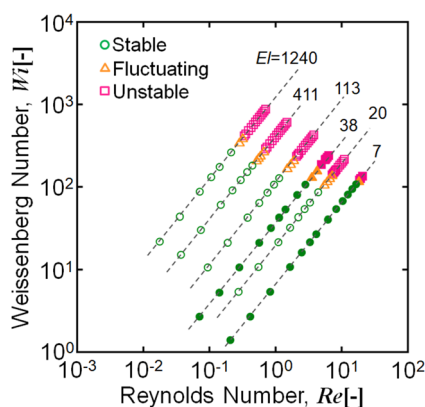


FIG. 6. Wi - Re phase diagram of Na-HA PBS solution in each channel. The open symbols show the experimental data measured in channels (A)–(C). Each El depends only on Na-HA concentration. $El = 20, 113, 411$, and 1240 correspond to the concentrations of 0.15, 0.25, 0.35, and 0.45 wt. %, respectively [in channels (A)–(C)]. The solid symbols show the results of channel (D). El was calculated as 7, 38, 137, and 412, which corresponds to the concentrations of 0.15, 0.25, 0.35, and 0.45 wt. %, respectively [in channel (D)]. $El = 137$ and 412 are not shown in the figure because these data overlap with the data of $El = 113$ and 411 of channels (A)–(C).

The width of the contraction throat of channels (A)–(C) is the same; therefore, both Re and Wi of a certain solution at identical flow rates are similar in these channels. Thus, El calculated for channels (A)–(C) is represented by a single line on the Wi - Re diagram, which only depends on the concentration of the solution. The width of the contraction part of channel (D) is different from the other channels; thus, El is also different from the other channels. The flow development along the line of El is represented by the following successive stages: Newtonian-like stable flow, lip vortices, stable corner vortices, time-dependent fluctuating corner vortices, and elastic instability. In the case of Na-HA PBS solution, stable, fluctuating, and unstable flow regimes were relatively well separated, as shown in Fig. 6. Here, Newtonian-like laminar flow, lip vortices, and stable corner vortices are categorized in the same stable flow regime, time-dependent fluctuating corner vortices are categorized in the fluctuating flow regime, and elastic instability is categorized in the unstable flow regime. The flow regimes in channels (A)–(C) were similar at each El ; therefore, the results of channels (A)–(C) can be combined. The flow behavior of channel (D) also shows similar tendency.

In the case of Na-HA water solution, stable, fluctuating, and unstable areas depend on the studied channel. Although the elasticity numbers of each solution are the same in channels (A)–(C), the transition borders are considerably different. Therefore, Fig. 7 shows only the critical points of the channels between the stable and transition flow regimes (shown by solid symbols) and between the fluctuating and unstable flow regimes (shown by open symbols). The short-dashed lines show El of channels (A), (B), and (C), which correspond to the flow rates measured in the experiments. The dotted-dashed lines show El of channel (D). As seen in Fig. 7, the critical points of these channels are different. The channel-dependent flow transition observed in Na-HA water solution may be affected by significantly higher El , compared with Na-HA PBS solution, and the rigidity of Na-HA in water solution.

To compare the flow regimes more precisely, the effects of the channel geometry on the flow regimes should be considered. In Fig. 8, the effects of contraction length L_c on the flow regimes of Na-HA water solutions at each El are summarized. Channels (A) and (C) have the same β and α , and different L_c . Figure 8 shows the flow

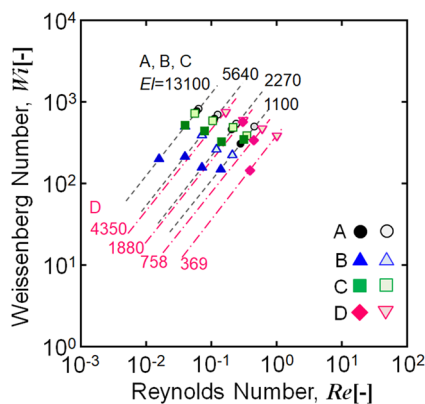


FIG. 7. Wi - Re phase diagram of Na-HA water solution in each channel. In the case of channels (A)–(C), $El = 1100, 2270, 5640$, and 13100 correspond to the concentrations of 0.15, 0.25, 0.35, and 0.45 wt. %, respectively. In the case of channel (D), $El = 369, 758, 1880$, and 4350 correspond to the concentrations of 0.15, 0.25, 0.35, and 0.45 wt. %, respectively. In this figure, only the critical points are plotted. Solid symbols (filled circles, filled triangles, filled squares, and filled diamonds) show the critical points from stable to fluctuating flow regimes. Open symbols (open circles, open triangles, open squares, and pink open diamonds) show the critical points from fluctuating to elastic instability flow regimes.

regimes of Na-HA water solutions at the concentrations from 0.15 to 0.45 wt. % which are semidilute-unentangled polymer solutions. In the case of 0.15 wt. % Na-HA water solution, the fluctuating flow occurs at similar Wi in both channels, and the unstable flow occurs

at lower Wi in channel (C), compared with channel (A). Almost all the Na-HA water solutions show similar tendencies to that observed in the case of 0.15 wt. % Na-HA water solution; namely, shorter L_c induced fluctuating and unstable flows at lower Wi . The increase in El due to the increase in the concentration did not affect the L_c effects.

In Fig. 9, the effects of L_c on the flow regimes of Na-HA PBS solutions at each El are summarized. In the figure, the flow regimes of Na-HA PBS solution at the concentrations from 0.15 to 0.45 wt. % are shown. Although 1.5 wt. % Na-HA PBS solution is a dilute polymer solution, 2.5–4.5 wt. % solutions are semidilute-entangled polymer solutions. In the case of 0.15 wt. % Na-HA PBS solution, the flow starts fluctuating at lower Wi in channel (C), but the unstable flow occurs at similar Wi in both channels. The tendency was similar to Na-HA water solution. However, in the cases of semidilute-entangled polymer solutions that are 0.25 wt. % to 0.45 wt. % solutions, the fluctuating and unstable flows occur at lower Wi in channel (A). The difference of L_c between channels (A) and (C) appeared to be small in terms of the transit times of the sample solutions and solution relaxation times.^{17,35} However, the effects of L_c on the flow regimes were observed, and the effects were varied by polymer entanglements.

In Fig. 10, the effects of β on the flow regimes of Na-HA water and PBS solutions are shown. Channels (A) and (D) have the same α and L_c , and different β . To compare the flow regimes of the water or PBS solutions at similar El in each channel, several solutions at different concentrations were studied. Here, the solutions in the unentangled regime and entangled regime were chosen, and it was checked whether the polymer entanglement changes the effects of β or not.

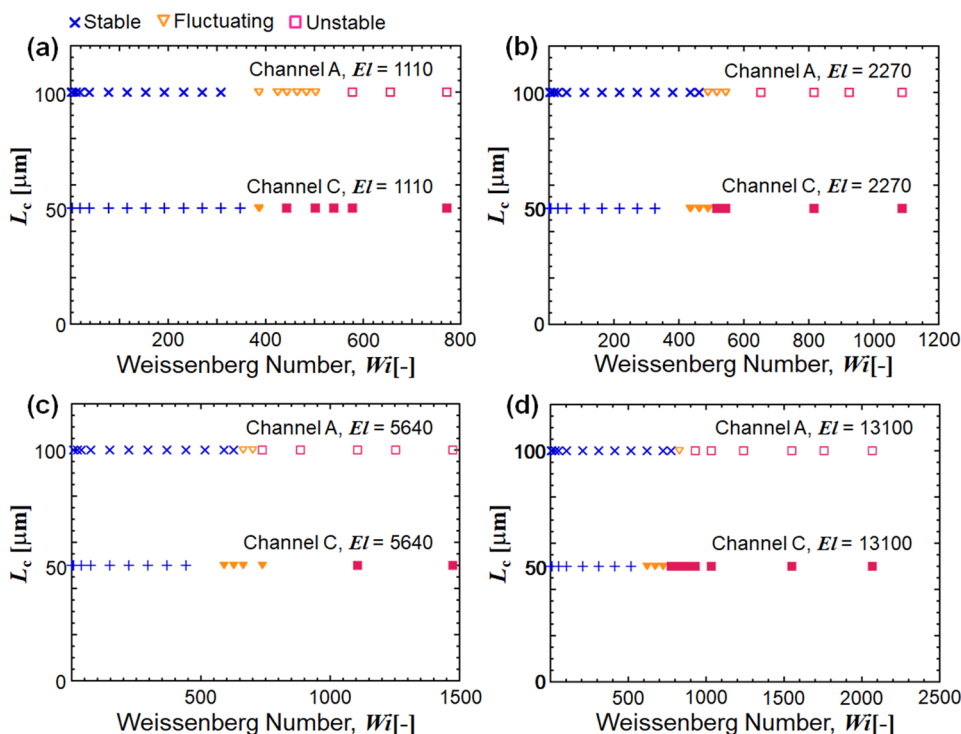


FIG. 8. Effects of L_c on the flow regimes of (a) 0.15 wt. %, (b) 0.25 wt. %, (c) 0.35 wt. %, and (d) 0.45 wt. % Na-HA water solution in each channel at each El .

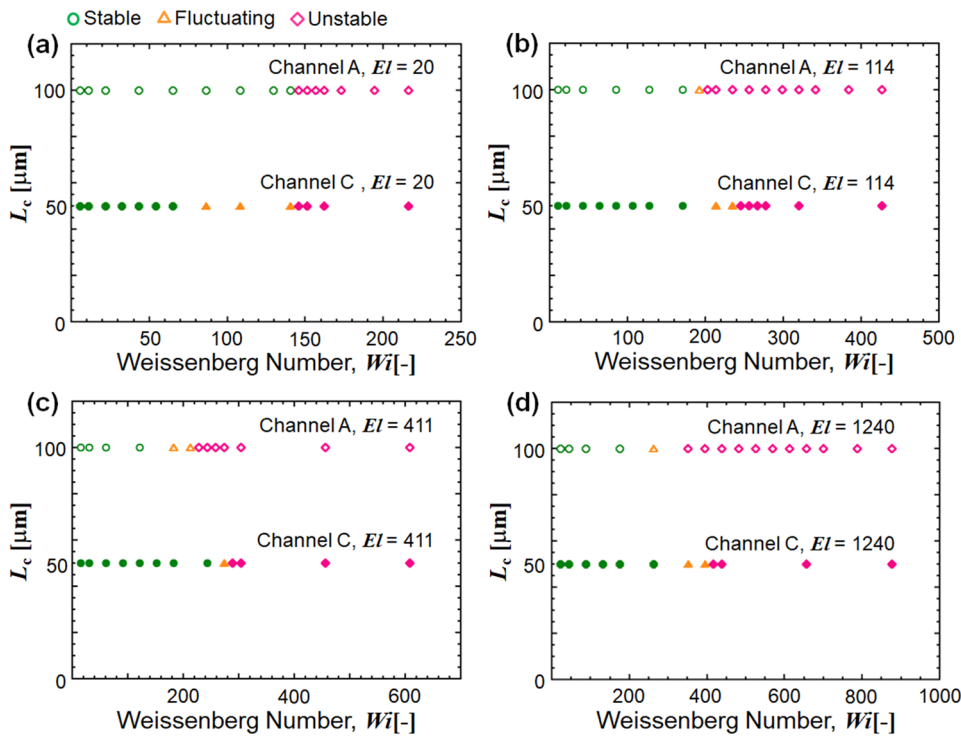


FIG. 9. Effects of L_c on the flow regimes of (a) 0.15 wt. %, (b) 0.25 wt. %, (c) 0.35 wt. %, and (d) 0.45 wt. % Na-HA PBS solutions in each channel at each EI .

In Fig. 10(a), the flow regimes of 0.15 wt. % Na-HA water solution in channel (A) and that of 0.3 wt. % Na-HA water solution in channel (D) are compared; in Fig. 10(b), the flow regimes of 0.25 wt. % Na-HA water solution and that of 0.4 wt. % Na-HA

water solution in each channel are compared. All these solutions are dilute or semidilute-unentangled solution. In Fig. 10(a), the fluctuating regimes occurred at lower Wi in channel (D), compared with channel (A); in Fig. 10(b), the fluctuating regimes occurred

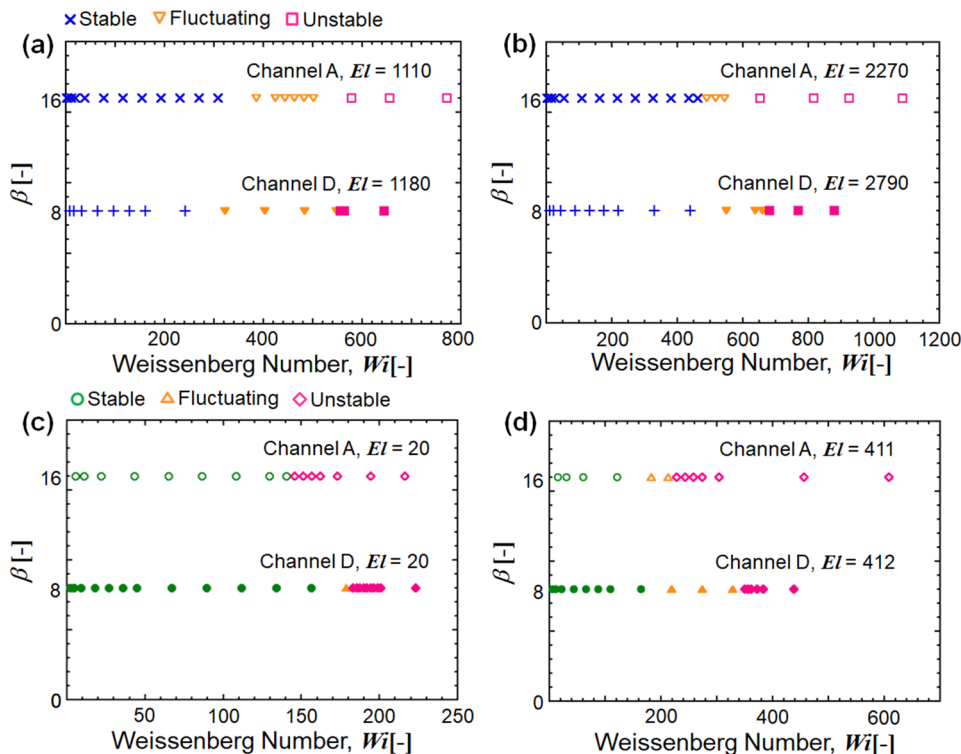


FIG. 10. Effects of β on the flow regimes of Na-HA water and PBS solutions. (a) 0.15 wt. % Na-HA water solution in channel (A) and 0.3 wt. % Na-HA water solution in channel (D). (b) 0.25 wt. % and 0.4 wt. % Na-HA water solutions in each channel. (c) 0.15 wt. % and 0.2 wt. % Na-HA PBS solutions in each channel. (d) 0.35 wt. % and 0.45 wt. % Na-HA PBS solutions in each channel.

at higher Wi in channel (D); the unstable flow started at almost the same Wi in both channels. In Fig. 10(c), the flow regimes of 0.15 wt. % Na-HA PBS solution in channel (A) and that of 0.2 wt. % Na-HA PBS solution in channel (D) are compared; these solutions are semidilute-unentangled solution. In Fig. 10(d), 0.35 wt. % and 0.45 wt. % Na-HA PBS solutions are compared; these solutions are semidilute-entangled solutions. In both cases of Na-HA PBS solution, the fluctuating and unstable flows occurred at higher Wi in channel (D). When the values of El were close to each other, higher β was likely to induce unstable flows at lower Wi . The effect of β obtained in the present study is consistent with the previous studies observing flexible polymer solutions.³² It was also found that the polymer entanglement did not change the effects of β .

In Fig. 11, the effects of α on the flow regimes of Na-HA water and PBS solutions are shown. Channels (B) and (D) have the same β and L_c , and different α . In Fig. 11(a), the flow regimes of 0.15 wt. % Na-HA water solution in channel (B) and those of 0.3 wt. % Na-HA water solution in channel (D) are compared; in Fig. 11(b), the flow regimes of 0.25 wt. % Na-HA water solution in each channel are compared. All these solutions are dilute or semidilute-unentangled solutions, and El in each comparison is close. In Fig. 11(c), the flow regimes of 0.15 wt. % Na-HA PBS solution in channel (B) and those of 0.2 wt. % Na-HA PBS solution in channel (D) are compared. PBS solutions at these concentrations are dilute solutions. In Fig. 11(d), the flow regimes of 0.35 wt. % Na-HA PBS solution and those of 0.45 wt. % Na-HA PBS solution in each channel are compared. PBS solutions at these concentrations are semidilute-entangled solutions. In all cases, higher α

induced the unstable flow regime at lower Wi . The results confirm the effect of α on the unstable flows, which was suggested in the previous studies.³⁶ It was also found that the polymer entanglement did not change the effects of α .

To clarify the effect of polymer entanglement on the flow regimes, we compare the flow regimes of 0.2 wt. % Na-HA water solution and that of 0.45 wt. % Na-HA PBS solution in channel (A). 0.2 wt. % Na-HA water solution is a semidilute-unentangled solution, and 0.45 wt. % PBS solution is a semidilute-entangled solution; Na-HA is more flexible in PBS solution. The relaxation time and shear viscosity of these solutions are almost the same; thus, the values of El are also very close. As shown in Fig. 12, although the values of El of these solutions are very close, the flow regimes are significantly different at similar Wi . The unstable flow was observed in 0.45 wt. % Na-HA PBS solution at lower Wi , which suggests that the polymer entanglement affects the flow regimes.

It has been proposed that many factors affect the flow regimes beyond channel geometry, including the relaxation time, rigidity of polymer molecules, and polymer entanglement. In this study, the Na-HA flexibility and relaxation time were controlled by varying the concentration and solvent. Then, the effects of the channel geometry on the flow regime were precisely compared. The effects of the channel geometry on the flow of an unentangled solution of flexible or semiflexible Na-HA were similar to the results obtained by previous studies, where dilute solutions of flexible polymers were observed. However, the semidilute-entangled solution of flexible Na-HA sometimes changed the flow beyond channel geometry and El (Figs. 9 and 12). As seen in the difference between Figs. 9(a) and

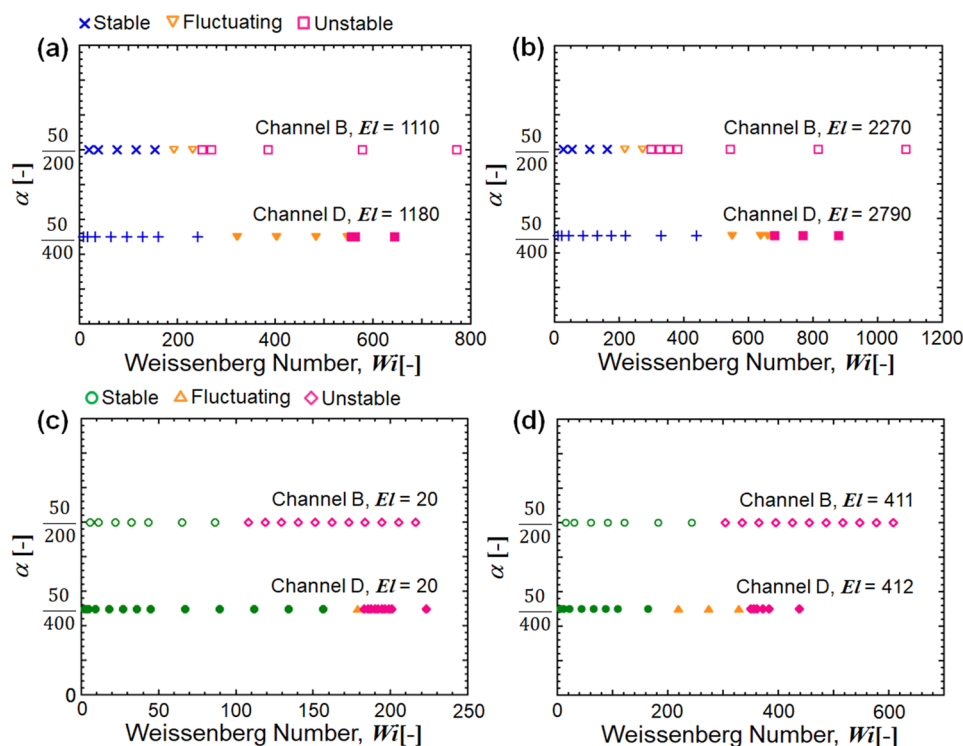


FIG. 11. Effects of α on the flow regimes of Na-HA water and PBS solutions. (a) 0.15 wt. % Na-HA water solution in channel (B) and 0.3 wt. % Na-HA water solution in channel (D). (b) 0.25 wt. % and 0.4 wt. % Na-HA water solutions in each channel. (c) 0.15 wt. % and 0.2 wt. % Na-HA PBS solutions in each channel. (d) 0.35 wt. % and 0.45 wt. % Na-HA PBS solutions in each channel.

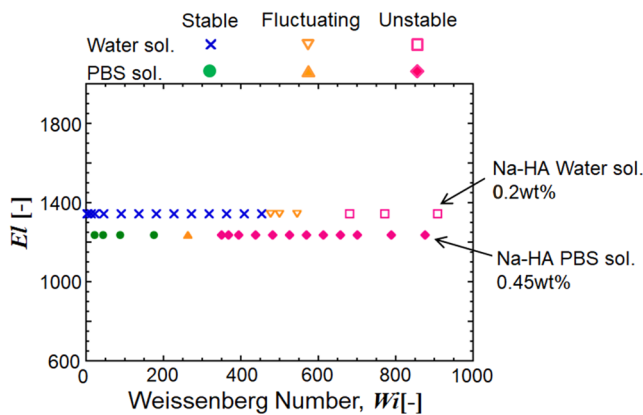


FIG. 12. Effects of the polymer entanglement on the flow regimes of Na-HA water and PBS solutions in channel (A).

9(b)–9(d), when the flow regime alteration was observed, the polymer entanglement was required. Therefore, we propose that polymer entanglement is a more dominant factor affecting the flow regimes, when compared with the relaxation time and polymer rigidity.

IV. CONCLUSION

In the present study, the flow characteristics of Na-HA solutions in planar abrupt contraction-expansion microchannels have been measured to clarify the effects of polymer flexibility and entanglement on the flow. As the ionic strength affects the rigidity of Na-HA, it is possible to vary the flexibility of the Na-HA molecules by changing the solvents. In particular, Na-HA is a semiflexible polymer when dissolved in water and flexible polymer when dissolved in PBS. The overlap concentration and entanglement concentration of these solutions were found by the viscosity measurements and by the analysis of the scaling index. Na-HA PBS solutions had the properties of a dilute, semidilute-unentangled, or semidilute-entangled solution depending on the concentration. Na-HA water solutions were practically in the range of semidilute-unentangled solutions at all the concentrations.

With the increasing flow rate, the following flow regimes of the Na-HA solutions in planar microchannels were observed: Newtonian-like laminar flow, lip vortices, stable corner vortices, time-dependent fluctuating corner vortices, and elastic unstable flows. In the channels with the same aspect ratios α , the growth curve of the corner vortices collapsed into almost a single linear curve. Then, the flow regimes were categorized as stable, fluctuating, and unstable flow regimes, which were summarized in Re – Wi space. In the case of Na-HA PBS solutions, the border between the stable and fluctuating flow regimes and the border between the fluctuating and unstable flow regimes in Re – Wi space in each channel were relatively close when the values of El were similar. However, in the case of Na-HA water solutions, the border in Re – Wi space was affected by the channel geometry. The rigidity of Na-HA in water solution and significantly higher El affect the flow regimes.

To quantify the effects of channel geometry (L_c , β , α) on the flow, the flow regimes were compared at different Wi and similar El . The effect of L_c on the flow of dilute or semidilute-unentangled

solution observed in the present study was similar to the previous studies with a highly flexible polymer, namely, shorter L_c induced fluctuating and unstable flows at lower Wi . However, the effects of L_c were varied by polymer entanglements. The effects of β and α observed in the present study are similar to the results obtained with flexible polymers, which were not altered by polymer entanglement. Then, the flow regimes of Na-HA semidilute-unentangled water solution and semidilute-entangled PBS solution at similar El in the same channel were compared. The Na-HA entanglement in the solution induced the flow transition at lower Wi . Although many factors, such as the channel geometry, relaxation time, rigidity of polymer molecules, and polymer entanglement, affect the flow regimes, when the flow regime alteration was observed, the polymer entanglement was an important factor in the present study. Therefore, it is suggested that the polymer entanglement is the dominant factor affecting the flow. Thus, the relatively flexible semidilute-entangled Na-HA PBS solution induces the flow transition at lower Wi .

In the present study, we extracted the effects of polymer flexibility and entanglement of Na-HA on the flow in microchannels. Although the effects of flexibility and entanglement on the elastic instability have not been completely clarified, the present study showed that Na-HA is a useful biopolymer for studying these effects because its rigidity and entanglement are possible to control by changing the ionic strength and solution concentration. Na-HA is also an important biopolymer in terms of medical applications, and abrupt contraction-expansion microchannels can provide useful information on the Na-HA solution properties.

ACKNOWLEDGMENTS

We gratefully acknowledge the Japan Society for the Promotion of Science (JSPS KAKENHI) for support of this research under a Grant-in-Aid for Young Scientists (A) (Project No.: 15H05552). We would also like to thank Tadashi Inoue at Osaka University for fruitful discussion about polymer entanglement.

REFERENCES

- P. J. Cable and D. V. Boger, "A comprehensive experimental investigation of tubular entry flow of viscoelastic fluids: Part I. Vortex characteristics in stable flow," *AIChE J.* **24**, 869 (1978).
- P. J. Cable and D. V. Boger, "A comprehensive experimental investigation of tubular entry flow of viscoelastic fluids: Part II. The velocity field in stable flow," *AIChE J.* **24**, 992 (1978).
- P. J. Cable and D. V. Boger, "A comprehensive experimental investigation of tubular entry flow of viscoelastic fluids: Part III. Unstable flow," *AIChE J.* **25**, 152 (1979).
- S. A. White, A. D. Gotsis, and D. G. Baird, "Review of the entry flow problem: Experimental and numerical," *J. Non-Newtonian Fluid Mech.* **24**, 121 (1987).
- D. V. Boger, D. U. Hur, and R. J. Binnington, "Further observations of elastic effects in tubular entry flows," *J. Non-Newtonian Fluid Mech.* **20**, 31 (1986).
- R. E. Evans and K. Walters, "Further remarks on the lip-vortex mechanism of vortex enhancement in planar-contraction flows," *J. Non-Newtonian Fluid Mech.* **32**, 95 (1989).
- D. V. Boger, "Viscoelastic flows through contractions," *Annu. Rev. Fluid Mech.* **19**, 157 (1987).
- D. V. Boger and R. J. Binnington, "Circular entry flows of fluid M1," *J. Non-Newtonian Fluid Mech.* **35**, 339 (1990).

- ⁹K. Chiba, T. Sakatani, and K. Nakamura, "Anomalous flow patterns in viscoelastic entry flow through a planar contraction," *J. Non-Newtonian Fluid Mech.* **36**, 193 (1990).
- ¹⁰K. Chiba, S. Tanaka, and K. Nakamura, "The structure of anomalous entry flow patterns through a planar contraction," *J. Non-Newtonian Fluid Mech.* **42**, 315 (1992).
- ¹¹J. P. Rothstein and G. H. McKinley, "Extensional flow of a polystyrene Boger fluid through a 4 : 1 : 4 axisymmetric contraction/expansion," *J. Non-Newtonian Fluid Mech.* **86**, 61 (1999).
- ¹²J. P. Rothstein and G. H. McKinley, "The axisymmetric contraction-expansion: The role of extensional rheology on vortex growth dynamics and the enhanced pressure drop," *J. Non-Newtonian Fluid Mech.* **98**, 33 (2001).
- ¹³H. Nguyen and D. V. Boger, "The kinematics and stability of die entry flows," *J. Non-Newtonian Fluid Mech.* **5**, 353 (1979).
- ¹⁴L. E. Rodd, T. P. Scott, D. V. Boger, J. J. Cooper-White, and G. H. McKinley, "The inertio-elastic planar entry flow of low-viscosity elastic fluids in micro-fabricated geometries," *J. Non-Newtonian Fluid Mech.* **129**, 1 (2005).
- ¹⁵L. E. Rodd, J. J. Cooper-White, D. V. Boger, and G. H. McKinley, "Role of the elasticity number in the entry flow of dilute polymer solutions in micro-fabricated contraction geometries," *J. Non-Newtonian Fluid Mech.* **143**, 170 (2007).
- ¹⁶E. Miller and J. J. Cooper-White, "The effects of chain conformation in the microfluidic entry flow of polymer-surfactant systems," *J. Non-Newtonian Fluid Mech.* **160**, 22 (2009).
- ¹⁷L. E. Rodd, D. Lee, K. H. Ahn, and J. J. Cooper-White, "The importance of downstream events in microfluidic viscoelastic entry flows: Consequences of increasing the constriction length," *J. Non-Newtonian Fluid Mech.* **165**, 1189 (2010).
- ¹⁸X. Hu, P. E. Boukany, O. L. Hemminger, and L. J. Lee, "The use of microfluidics in rheology," *Macromol. Mater. Eng.* **296**, 308 (2011).
- ¹⁹S. J. Haward, T. J. Ober, M. S. N. Oliveira, M. A. Alves, and G. H. McKinley, "Extensional rheology and elastic instabilities of a wormlike micellar solution in a microfluidic cross-slot device," *Soft Matter* **8**, 536 (2012).
- ²⁰S. J. Haward, G. H. McKinley, and A. Q. Shen, "Elastic instabilities in planar elongational flow of monodisperse polymer solutions," *Sci. Rep.* **6**, 33029 (2016).
- ²¹A. Groisman and S. R. Quake, "A microfluidic rectifier: Anisotropic flow resistance at low Reynolds numbers," *Phys. Rev. Lett.* **92**, 094501 (2004).
- ²²C. J. Pipe and G. H. McKinley, "Microfluidic rheometry," *Mech. Res. Commun.* **36**, 110 (2009).
- ²³T. J. Ober, S. J. Haward, C. J. Pipe, J. Soulages, and G. H. McKinley, "Microfluidic extensional rheometry using a hyperbolic contraction geometry," *Rheol. Acta* **52**, 529 (2013).
- ²⁴H. S. Lee and S. J. Muller, "A differential pressure extensional rheometer on a chip with fully developed elongational flow," *J. Rheol.* **61**, 1049 (2017).
- ²⁵S. G. Kim, C. M. Ok, and H. S. Lee, "Steady-state extensional viscosity of a linear polymer solution using a differential pressure extensional rheometer on a chip," *J. Rheol.* **62**, 1261 (2018).
- ²⁶S. Nigen and K. Walters, "Viscoelastic contraction flows: Comparison of axisymmetric and planar configurations," *J. Non-Newtonian Fluid Mech.* **102**, 343 (2002).
- ²⁷M. A. Alves, P. J. Oliveira, and F. T. Pinho, "On the effect of contraction ratio in viscoelastic flow through abrupt contractions," *J. Non-Newtonian Fluid Mech.* **122**, 117 (2004).
- ²⁸M. A. Alves, F. T. Pinho, and P. J. Oliveira, "Visualizations of Boger fluid flows in a 4:1 square-square contraction," *AIChE J.* **51**, 2908 (2005).
- ²⁹P. C. Sousa, P. M. Coelho, M. S. N. Oliveira, and M. A. Alves, "Three-dimensional flow of Newtonian and Boger fluids in square-square contractions," *J. Non-Newtonian Fluid Mech.* **160**, 122 (2009).
- ³⁰R. Hidema, T. Shiraki, Y. Tanino, Y. Komoda, and H. Suzuki, "Extensional viscosity of low viscous polymer solutions measured by pressure drops in abrupt contraction channels," *J. Soc. Rheol., Jpn.* **46**, 13 (2018).
- ³¹S. Gulati, S. J. Muller, and D. Liepmann, "Direct measurements of viscoelastic flows of DNA in a 2:1 abrupt planar micro-contraction," *J. Non-Newtonian Fluid Mech.* **155**, 51 (2008).
- ³²S. J. Haward, Z. Li, D. Lighter, B. Thomas, J. A. Odell, and X.-F. Yuan, "Flow of dilute to semi-dilute polystyrene solutions through a benchmark 8:1 planar abrupt micro-contraction," *J. Non-Newtonian Fluid Mech.* **165**, 1654 (2010).
- ³³S. C. Omowunmi and X.-F. Yuan, "Modelling the three-dimensional flow of a semi-dilute polymer solution in microfluidics—on the effect of aspect ratio," *Rheol. Acta* **49**, 585 (2010).
- ³⁴S. C. Omowunmi and X.-F. Yuan, "Time-dependent non-linear dynamics of polymer solutions in microfluidic contraction flow—a numerical study on the role of elongational viscosity," *Rheol. Acta* **52**, 337 (2013).
- ³⁵Z. Li, X.-F. Yuan, S. J. Haward, J. A. Odell, and S. Yeates, "Non-linear dynamics of semi-dilute polydisperse polymer solutions in microfluidics: A study of a benchmark flow problem," *J. Non-Newtonian Fluid Mech.* **166**, 951 (2011).
- ³⁶A. Lanzaro and X.-F. Yuan, "Effects of contraction ratio on non-linear dynamics of semi-dilute, highly polydisperse PAAm solutions in microfluidics," *J. Non-Newtonian Fluid Mech.* **166**, 1064 (2011).
- ³⁷A. Lanzaro and X.-F. Yuan, "A quantitative analysis of spatial extensional rate distribution in nonlinear viscoelastic flows," *J. Non-Newtonian Fluid Mech.* **207**, 32 (2014).
- ³⁸U. A. Klebetainger, B. K. Wunderlich, and A. R. Bausch, "Transient flow behavior of complex fluids in microfluidic channels," *Microfluid. Nanofluid.* **15**, 533 (2013).
- ³⁹D. Lee and K. H. Ahn, "Time-Weissenberg number superposition in planar contraction microchannel flows," *J. Non-Newtonian Fluid Mech.* **210**, 41 (2014).
- ⁴⁰P. Pakdel and G. H. McKinley, "Elastic instability and curved streamlines," *Phys. Rev. Lett.* **77**, 2459 (1996).
- ⁴¹G. H. McKinley, P. Pakdel, and A. Öztekin, "Rheological and geometric scaling of purely elastic flow instabilities," *J. Non-Newtonian Fluid Mech.* **67**, 19 (1996).
- ⁴²S. Kenney, K. Poper, G. Chapagain, and G. F. Christopher, "Large Deborah number flows around confined microfluidic cylinders," *Rheol. Acta* **52**, 485 (2013).
- ⁴³X. Shi, S. Kenney, G. Chapagain, and G. F. Christopher, "Mechanisms of onset for moderate Mach number instabilities of viscoelastic flows around confined cylinders," *Rheol. Acta* **54**, 805 (2015).
- ⁴⁴S. J. Haward, J. Page, T. A. Zaki, and A. Q. Shen, "'Phase diagram' for viscoelastic Poiseuille flow over a wavy surface," *Phys. Fluids* **30**, 113101 (2018).
- ⁴⁵N. Burshtein, A. Q. Shen, and S. J. Haward, "Controlled symmetry breaking and vortex dynamics in intersecting flows," *Phys. Fluids* **31**, 034104 (2019).
- ⁴⁶R. E. Evans and K. Walters, "Flow characteristics associated with abrupt changes in geometry in the case of highly elastic liquids," *J. Non-Newtonian Fluid Mech.* **20**, 11 (1986).
- ⁴⁷M. A. Alves, P. J. Oliveira, and F. T. Pinho, "Benchmark solutions for the flow of Oldroyd-B and PTT fluids in planar contractions," *J. Non-Newtonian Fluid Mech.* **110**, 45 (2003).
- ⁴⁸L. Martin-Alarcon and T. A. Schmidt, "Rheological effects of macromolecular interactions in synovial fluid," *Biorheology* **53**, 49 (2016).
- ⁴⁹M. K. Cowman and S. Matsuoka, "Experimental approaches to hyaluronan structure," *Carbohydr. Res.* **340**, 791 (2005).
- ⁵⁰M. K. Cowman, T. A. Schmidt, P. Raghavan, and A. Stecco, "Viscoelastic properties of hyaluronan in physiological conditions," *F1000Research* **4**, 622 (2015).
- ⁵¹W. E. Krause, E. G. Bellomo, and R. H. Colby, "Rheology of sodium hyaluronate under physiological conditions," *Biomacromolecules* **2**, 65 (2001).
- ⁵²T. Sato, S. Yamamoto, T. Takigawa, and T. Masuda, "Zero-shear viscosity of aqueous solutions of sodium hyaluronate: Analysis as semiflexible polymer solutions," *J. Soc. Rheol., Jpn.* **29**, 204 (2001) (in Japanese).
- ⁵³A. Ö. Bingöl, D. Lohmann, K. Püschel, and W.-M. Kulicke, "Characterization and comparison of shear and extensional flow of sodium hyaluronate and human synovial fluid," *Biorheology* **47**, 205 (2010).
- ⁵⁴S. J. Haward, "Characterization of hyaluronic acid and synovial fluid in stagnation point elongational flow," *Biopolymers* **101**, 287 (2013).
- ⁵⁵S. J. Haward, "Synovial fluid response to extensional flow: Effects of dilution and intermolecular interactions," *PLoS One* **9**, e92867 (2014).

- ⁵⁶K. Hayashi, K. Tsutsumi, F. Nakajima, T. Norisuye, and A. Teramoto, "Chain-stiffness and excluded-volume effects in solutions of sodium hyaluronate at high ionic strength," *Macromolecules* **28**, 3824 (1995).
- ⁵⁷K. Tsutsumi and T. Norisue, "Excluded-volume effects in sodium hyaluronate solutions revisited," *Polym. J.* **30**, 345 (1998).
- ⁵⁸E. Weiss, K. Groenen-Serrano, and A. Savall, "Electrochemical mineralization of sodium dodecylbenzenesulfonate at boron doped diamond anodes," *J. Appl. Electrochem.* **37**, 1337 (2007).
- ⁵⁹S. W. H. Shah, B. Naseem, W. Rehman, N. Bashir, and S. S. Shah, "Investigation of 1-alkanols in organised solutions," *Bull. Chem. Soc. Ethiop.* **25**, 469 (2011).
- ⁶⁰G. H. McKinley and A. Tripathi, "How to extract the Newtonian viscosity from capillary breakup measurements in a filament rheometer," *J. Rheol.* **44**, 653 (2000).
- ⁶¹L. R. Rodd, T. P. Scott, J. J. Cooper-White, and G. H. McKinley, "Capillary break-up rheometry of low-viscosity elastic fluids," *Appl. Rheol.* **15**, 12 (2005).
- ⁶²M. I. Kolte and P. Szabo, "Capillary thinning of polymeric filaments," *J. Rheol.* **43**, 609 (1999).
- ⁶³L. A. Shelley and G. H. McKinley, "Elasto-capillary thinning and breakup of model elastic liquids," *J. Rheol.* **45**, 115 (2001).
- ⁶⁴G. H. McKinley, HML Preprint No. 05-P-04, 2005.